ACS OMEGA

http://pubs.acs.org/journal/acsodf

Article

Highly Stable Supramolecular Donor–Acceptor Complexes Involving a Bis(18-Crown-6)azobenzene as Weak Donor: Structure–Property Relationships

Evgeny N. Ushakov,* Timofey P. Martyanov, Artem I. Vedernikov, Asya A. Efremova, Anna A. Moiseeva, Lyudmila G. Kuz'mina, Svetlana N. Dmitrieva, Judith A. K. Howard, and Sergey P. Gromov*

Cite This: *ACS Omega* 2020, 5, 25993–26004

Read Online

ACCESS | Metrics & More | Article Recommendations | Supporting Information

ABSTRACT: The physicochemical properties of highly stable supramolecular donor–acceptor (D–A) complexes of a bis(18-crown-6)azobenzene (weak π-donor) with a series of bis(ammonioalkyl) derivatives of viologen-like molecules (π-acceptors) in acetonitrile were studied using cyclic voltammetry, UV–vis absorption spectroscopy, ^{1}H NMR spectroscopy, and density functional theory (DFT) calculations. The crystalline structures of the bis(crown)azobenzene and its complex with a bis(ammoniopropyl) derivative of 2,7-diazapyrene were determined by X-ray diffraction analysis. In solution, all of the supramolecular D–A complexes studied have a pseudocyclic structure owing to ditopic coordination of the ammonium groups of the acceptor to the crown ether moieties of the donor. These complexes show somewhat lower stability as compared with the previously studied complexes of the related derivative of stilbene (strong π-donor), which is explained by the relatively weak intermolecular charge-transfer (CT) interactions. Time-dependent DFT calculations predict that the low-energy CT transition in the D–A complex of the bis(crown)azobenzene with a bis(ammoniopropyl) derivative of 4,4′-bipyridine lies between the local $\pi\pi^*$ and $n\pi^*$ transitions of the azobenzene. The absorption band associated with the CT transition is indiscernible in the spectrum since it is overlapped with broad and more intense $\pi\pi^*$ and $n\pi^*$ bands. It was found that the $E \rightarrow Z$ photoisomerization quantum yield of the bis(crown)azobenzene decreases by almost an order of magnitude upon the complexation with the 4,4′-bipyridine derivative. This effect was tentatively attributed to the intermolecular electron transfer that occurs in the $^1\pi\pi^*$ excited state of the azobenzene and competes with the $^1\pi\pi^* \rightarrow {}^1n\pi^*$ internal conversion.

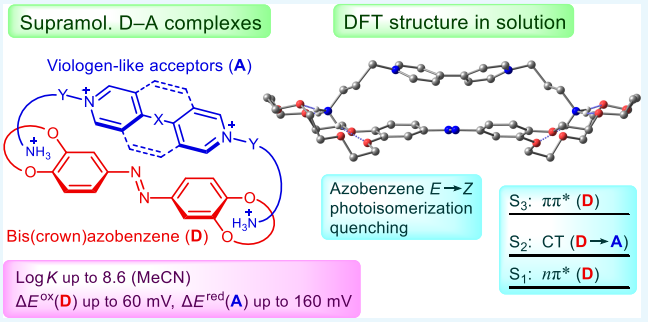

1. INTRODUCTION

Organic electron donor–acceptor (D–A) complexes in which the charge-transfer (CT) electronic transition occurs at a lower energy than the local transitions of the donor and the acceptor are commonly called CT complexes. They are used in various fields of materials science and chemistry, such as the development of organic solar cells,[1] field-effect transistors,[2,3] and "off–on" fluorescent sensors,[4] as model systems for studying ultrafast electron-transfer reactions[5] and as artificial light-harvesting antenna models.[6−8] CT complexes play important roles in biological systems;[9−12] the examples are DNA UV-damage repair[13] and magnetic field sensing.[14] The formation of CT complexes can be observed upon the interaction of biomolecules with drugs.[15−17]

In solutions, organic D–A complexes normally show a very low thermodynamic stability and, therefore, cannot be observed at low concentrations of the components. This problem can be solved by using molecular self-assembly methods. Previously, we reported on a comprehensive study of complexes of bis(18-crown-6)stilbene (*E*)-**1** (strong electron donor) with viologen-like compounds (electron acceptors) containing two ammonioalkyl groups (Scheme 1).[4,5,18,19] These D–A complexes in MeCN solutions are characterized by very-high-stability constants ($K_{1:1}$ up to $10^{9.4}$ M^{-1}) due to ditopic coordination *via* hydrogen bonds and demonstrate low-intensity absorption bands in the visible region, associated with intermolecular CT electronic transitions.

Herein, we report the results of a study of similar supramolecular D–A complexes involving bis(18-crown-6)-azobenzene (*E*)-**2** that has a weaker electron-donating ability as compared with that of stilbene (*E*)-**1**.

Received: July 18, 2020
Accepted: September 15, 2020
Published: September 29, 2020

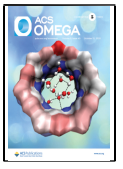

https://dx.doi.org/10.1021/acsomega.0c03441
ACS Omega 2020, 5, 25993–26004

Scheme 1. Formation of Supramolecular D−A Complexes Involving Stilbene (*E*)-1 or Azobenzene (*E*)-2 as the Electron Donor and Compounds (3−5)a,b as the Electron Acceptors; Chemical Structures of Reference Acceptors (*E*)-4c and 5c

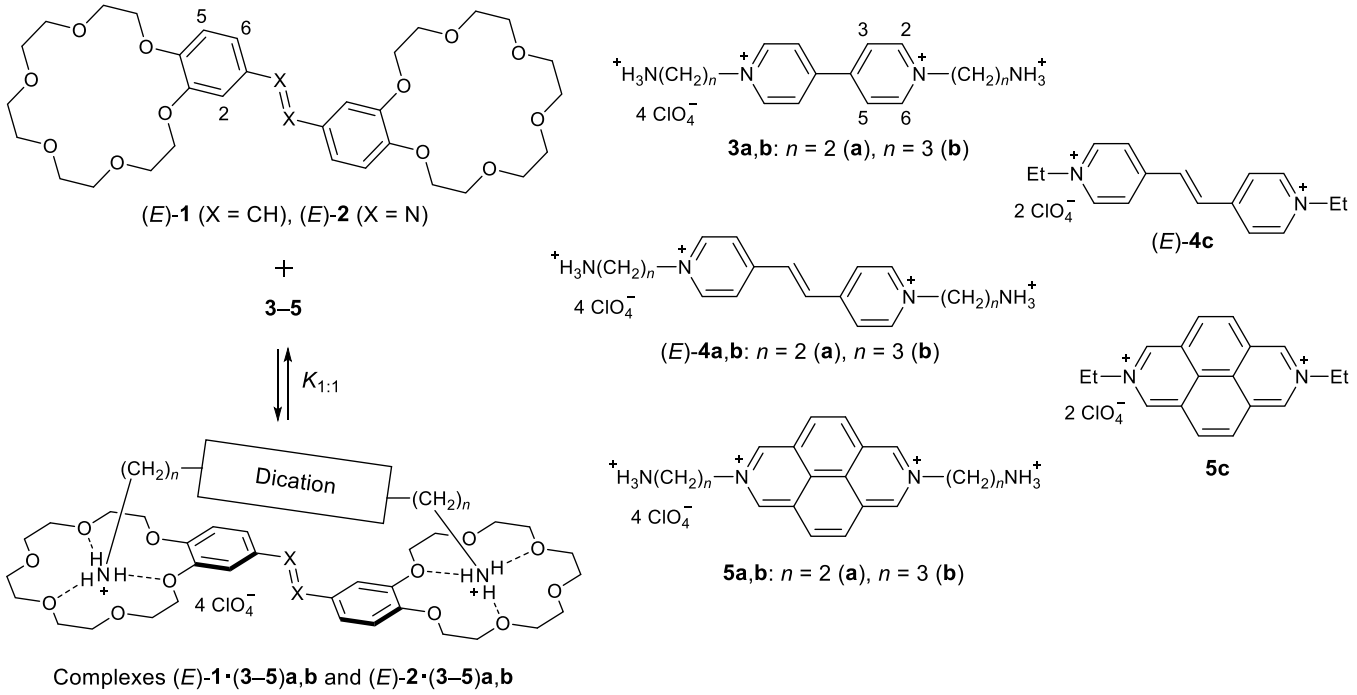

Azobenzene derivatives are used as molecular photoswitches in various fields,[20−26] in particular, in photopharmacology.[27−32] It was shown that the complexation of functionalized azobenzene derivatives with biologically active molecules can allow one to control the properties of the latter with light. Theoretically, the photoswitchable behavior and other properties of azobenzenes in complexes with molecules having strong electron-withdrawing moieties can be significantly influenced by intermolecular CT interactions. However, the magnitude of this influence is rather difficult to predict since donor−acceptor complexes involving azobenzene derivatives have not been studied.

2. RESULTS AND DISCUSSION

2.1. Redox Properties. The redox properties of azobenzene (*E*)-**2** and supramolecular complexes (*E*)-**2**·**3b** and (*E*)-**2**·(*E*)-**4a,b** were studied using cyclic voltammetry at a glassy carbon electrode in MeCN containing Bu_4NClO_4 (0.1 M). The cyclic voltammetry data for stilbene (*E*)-**1**, compounds **3b** and (*E*)-**4a,b**, and complexes (*E*)-**1**·**3b** and (*E*)-**1**·(*E*)-**4a,b** were reported previously.[4,33] The peak potentials of the first redox transitions, vs Ag|AgCl|KCl (aq, sat.), for all of these molecules and complexes are collected in Table 1. The cyclic voltammograms for azobenzene (*E*)-**2** and complexes (*E*)-**2**·**3b**, (*E*)-**2**·(*E*)-**4a**, and (*E*)-**2**·(*E*)-**4b** are presented in the Supporting Information (Figure S1).

The first oxidation potential of azobenzene (*E*)-**2** is 370 mV higher than that of stilbene (*E*)-**1**, which indicates a relatively weak electron-donating ability of (*E*)-**2**. The formation of pseudocyclic D−A complexes (Scheme 1) is accompanied by anodic shifts of the first oxidation potentials of (*E*)-**1** and (*E*)-**2**. This is explained by two factors:[4] first, the radical cations (*E*)-$\mathbf{1}^{\bullet+}$ and (*E*)-$\mathbf{2}^{\bullet+}$ complexed to the tetracationic acceptors are destabilized due to Coulomb repulsion and, second, the ammonium groups of the acceptor bound to the crown ether moieties of the donor exert an electron-withdrawing effect on the π-conjugated moiety of the donor. The anodic shift ΔE_p^{ox} varies from 190 to 240 mV for (*E*)-**1** and from 20 to 60 mV for (*E*)-**2**, depending on the acceptor structure. The lower values of ΔE_p^{ox} for azobenzene (*E*)-**2** suggest weaker CT interactions in the D−A complexes of this compound as compared with those for stilbene (*E*)-**1**.[33] This suggestion is in agreement with the data on the stability constants of D−A complexes, presented in Section 2.2.

The first reduction potentials of acceptors **3b** and (*E*)-**4a,b** are shifted to less negative values upon the complexation with donors (*E*)-**1** and (*E*)-**2**. The positive values of ΔE_p^{red} are tentatively attributed to significant changes in the solvation

Table 1. Peak Potentials of the First Redox Transitions for Electron Donors (*E*)-1 and (*E*)-2, Electron Acceptors 3b and (*E*)-4a,b, and Supramolecular D−A Complexes in MeCN[a]

species	E_p^{ox}, V	E_p^{red}, V	ΔE_p^{ox}, mV	ΔE_p^{red}, mV
(*E*)-**1**	1.0 rev[b]	−2.48[b]		
(*E*)-**2**	1.37	−1.57		
3b		−0.41 rev[c]		
(*E*)-**4a**		−0.50 rev[b]		
(*E*)-**4b**		−0.50 rev[b]		
(*E*)-**1**·**3b**	1.19[c]	−0.38 rev[c]	190	30
(*E*)-**1**·(*E*)-**4a**	1.24[b]	−0.43 rev[b]	240	70
(*E*)-**1**·(*E*)-**4b**	1.24[b]	−0.43 rev[b]	240	70
(*E*)-**2**·**3b**	1.42	−0.38 rev	50	30
(*E*)-**2**·(*E*)-**4a**	1.39	−0.34 rev	20	160
(*E*)-**2**·(*E*)-**4b**	1.43	−0.41 rev	60	90

[a]Supporting electrolyte Bu_4NClO_4 (0.1 M), glassy carbon electrode vs Ag|AgCl|KCl (aq, sat.), rev denotes reversible (the forward to reverse peak potential difference is about 60 mV), $\Delta E_p^{ox} = E_p^{ox}$(complex) − E_p^{ox}(free donor), $\Delta E_p^{red} = E_p^{red}$(complex) − E_p^{red}(free acceptor). [b]From ref 33. [c]From ref 4.

https://dx.doi.org/10.1021/acsomega.0c03441
ACS Omega 2020, 5, 25993−26004

shell of the charged acceptor molecule upon the formation of pseudocyclic D−A complexes and a specific interaction of the reduced form of the acceptor with the π-conjugated moiety of the donor.[4]

2.2. Photochemical Study. Figure 1 shows the absorption spectra of azobenzene (*E*)-**2** and its pseudocyclic complexes with 1,9-diammoniononane diperchlorate (**6**) and bis-ammonium bipyridine derivative **3b** in MeCN.

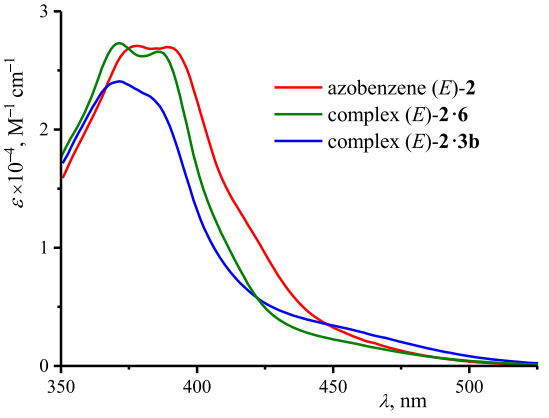

Figure 1. Absorption spectra of azobenzene (*E*)-**2** and its pseudocyclic complexes with diammonium compound **3b** and 1,9-diammoniononane diperchlorate (**6**) in MeCN.

The complex formation in both cases leads to a hypsochromic shift of the intense absorption band of (*E*)-**2** associated with the ππ* electronic transition, which is due to the electron-withdrawing effect of the ammonium ions bound to the crown ether fragments of (*E*)-**2** on the azobenzene moiety. In addition, the complexation with acceptor **3b** leads to a decrease in the intensity of the ππ* transition band and a discernible increase in the absorptivity at the long-wavelength edge of the spectrum. These effects are attributable to charge-transfer interaction and/or other specific interactions between the bipyridinium and azobenzene moieties of the complex, which result in a strong deviation from the planarity of the azobenzene moiety. The deviation from planarity causes a bathochromic shift and an increase in the intensity of the weak nπ* transition band of the azobenzene (see the results of density functional theory (DFT) calculations in Section 2.5).

Complex (*E*)-**2**·**3b** does not exhibit any CT absorption bands, in contrast to the related complex of stilbene (*E*)-**1**, which shows a clear-cut CT band with the maximum at 493 nm.[4] According to time-dependent DFT calculations (TD-DFT, Section 2.5), the CT transition (azobenzene-to-viologen) in the (*E*)-**2**·**3b** complex lies in the region between the local ππ* and nπ* transitions of the azobenzene and is characterized by a very low oscillator strength. Hence, the CT absorption band of (*E*)-**2**·**3b** is unobservable because it is overlapped with the broad and more intense bands associated with the ππ* and nπ* transitions.

The changes in the spectrum of (*E*)-**2** observed upon the complexation with acceptors **3a**, (*E*)-**4a**,**b**, and **5a**,**b** were similar to those observed in the case of viologen **3b**.

Table 2 shows the stability constants of the bimolecular pseudocyclic complexes of azobenzene (*E*)-**2** with acceptor molecules (**3**−**5**)**a**,**b** and diammonium compound **6** in MeCN. The reference data available for the corresponding complexes

Table 2. Stability Constants of the Bimolecular Complexes of (*E*)-1 and (*E*)-2 with Acceptor Molecules (3−5)a,b and Diammonium Compound 6[a]

	(*E*)-**1**	(*E*)-**2**
acceptor	$\log K_{1:1}$	$\log K_{1:1}$
3a	7.36[b]	7.0
3b	9.15[b]	8.2
(*E*)-**4a**	9.42[b]	8.6
(*E*)-**4b**	9.08[b]	8.2
5a	7.72[b]	6.9
5b	9.39[b]	8.4
6	6.78[c]	6.58

[a]In MeCN; $K_{1:1}$ = [D·A]/([D][A]), M^{-1}. [b]From ref 4. [c]From ref 18.

of stilbene (*E*)-**1** are presented for comparison in the same table.

The complexes of azobenzene (*E*)-**2** are characterized by a lower stability compared with the corresponding complexes of stilbene (*E*)-**1**. With diammonium compound **6**, the decrease in $\log K_{1:1}$ is as low as 0.2 and is attributable to the fact that in (*E*)-**2** the electron density on the crown ether oxygen atoms directly connected to the benzene rings is somewhat lower compared to (*E*)-**1**. In the case of acceptor molecules (**3**−**5**)**a**,**b**, the values of $\log K_{1:1}$ decrease more significantly (by 0.4−1.0), which indicates weaker CT interactions in the D−A complexes of azobenzene (*E*)-**2** in comparison with the corresponding complexes of stilbene (*E*)-**1**.

Figures 2 and 3 present the spectrophotometric data on the steady-state photolysis of azobenzene (*E*)-**2** and complex (*E*)-

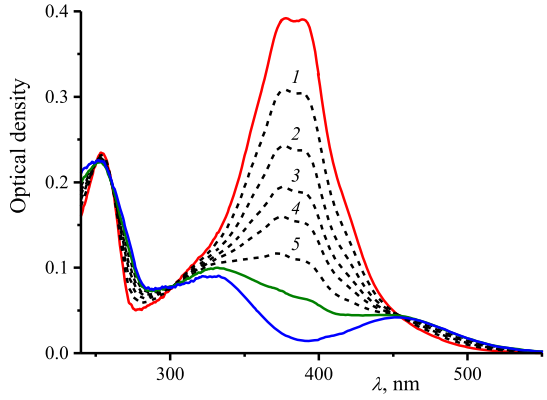

Figure 2. Spectrophotometric data on the steady-state photolysis of azobenzene (*E*)-**2** in MeCN with 365 nm light: 1 cm cell, concentration 1.5×10^{-5} M, light intensity 2×10^{-9} mol cm^{-2} s^{-1}. The red curve is the spectrum of (*E*)-**2**; the dashed curves are the spectra recorded after irradiation for (1) 10, (2) 20, (3) 30, (4) 40, and (5) 60 s; the olive curve is the spectrum of the *E*−*Z* photostationary state; and the blue curve is the approximated spectrum of (*Z*)-**2** (see Section 4.5).

2·**3b** in MeCN with 365 nm light. In both cases, the photoirradiation leads to a strong decrease in the intensity of the ππ* absorption band of the azobenzene and to an increase in the intensity of the long-wavelength nπ* absorption band. These spectral changes are due to the *E*−*Z* photoisomerization of (*E*)-**2**. The nπ* absorption band of (*Z*)-**2**·**3b** (λ_{max} = 456 nm) is shifted to the red by 4 nm relative to that of free (*Z*)-**2**.

The quantum yields of the forward and back *E*−*Z* photoisomerization reactions (φ_{E-Z} and φ_{Z-E}) of azobenzene

https://dx.doi.org/10.1021/acsomega.0c03441
ACS Omega 2020, 5, 25993−26004

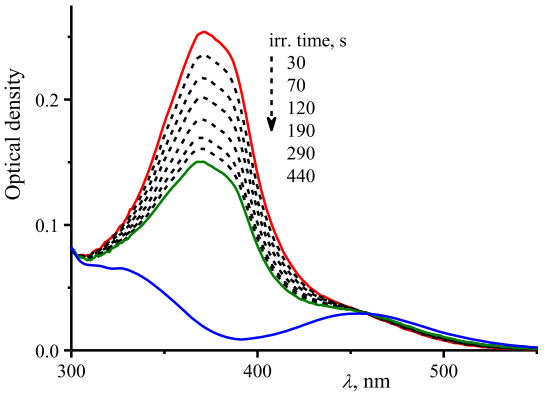

Figure 3. Spectrophotometric data on the steady-state photolysis of complex (*E*)-**2·3b** in MeCN with 365 nm light: 1 cm cell, concentration 1.0×10^{-5} M, light intensity 2×10^{-9} mol cm^{-2} s^{-1}. The red curve is the spectrum of (*E*)-**2·3b**; the olive curve is the spectrum of the *E*−*Z* photostationary state; and the blue curve is the approximated spectrum of (*Z*)-**2·3b** (see Section 4.5).

2 in the free form and as complexes **2·3b** and **2·6** are given in Table 3. The complex formation in both cases has almost no

Table 3. Quantum Yields of the Forward and Back *E*−*Z* Photoisomerization Reactions (φ_{E-Z} and φ_{Z-E}) of Azobenzene 2 in the Free Form and as Complexes 2·3b and 2·6 in MeCN

	φ_{E-Z}	φ_{Z-E}
2	0.22	0.32
2·6	0.17	0.31
2·3b	0.025	0.32

effect on φ_{Z-E}. The formation of complex (*E*)-**2·6** leads to a moderate decrease in φ_{E-Z}, which may arise from an electron-withdrawal influence of the ammonium ions on the azobenzene moiety of (*E*)-**2** and/or from steric hindrances for the photoisomerization in the pseudocyclic complex. The φ_{E-Z} quantum yield of (*E*)-**2** decreases almost by an order of magnitude upon the formation of complex (*E*)-**2·3b**. Presumably, this is due to the intermolecular electron transfer from (*E*)-**2** to **3b**, which occurs in the $^1\pi\pi^*$ excited state of the azobenzene and competes with the internal conversion to the $^1n\pi^*$ state (experimental and theoretical studies showed that the *E* → *Z* photoisomerization of unsubstituted azobenzene takes place in the $^1n\pi^*$ excited state following fast $^1\pi\pi^*$ → $^1n\pi^*$ internal conversion).[34−36]

2.3. NMR Spectroscopy Study. Bis(crown)azobenzene (*E*)-**2** is very similar in structure to bis(crown)stilbene (*E*)-**1**; therefore, the D−A complexes of (*E*)-**2** with diammonium compounds (**3**−**5**)**a**,**b** should be structurally analogous to the corresponding D−A complexes of (*E*)-**1**, which have been studied previously by ^{1}H NMR spectroscopy.[4,19]

Figures 4 and 5 show the aromatic and aliphatic regions of the ^{1}H NMR spectra of azobenzene (*E*)-**2**, viologen **3b**, and their equimolar mixture in MeCN-d_3. The equimolar mixing of (*E*)-**2** and **3b** leads to significant shifts of most proton signals of both compounds, which indicates the formation of a highly stable bimolecular complex owing to ditopic coordination of the ammonium groups of **3b** to the crown ether moieties of (*E*)-**2** (see Scheme 1). The equimolar mixing of (*E*)-**2** with other acceptor compounds from the series (**3**−**5**)**a**,**b** also

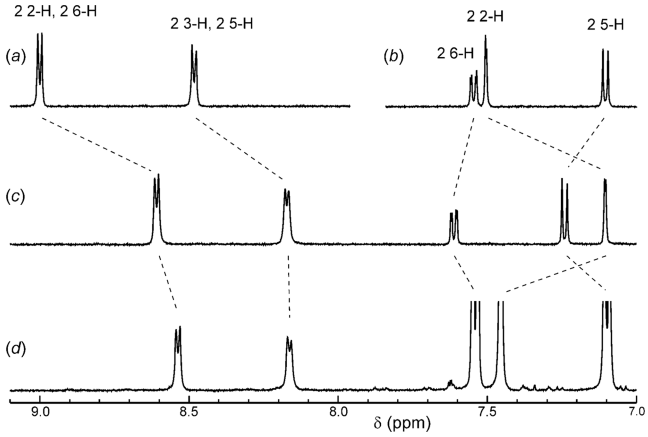

Figure 4. ^{1}H NMR spectra (aromatic region) of (a) viologen **3b** (1 mM), (b) azobenzene (*E*)-**2** (1 mM), (c) an equimolar mixture of **3b** and (*E*)-**2**, (d) a 1:10 mixture of **3b** and (*E*)-**2**; MeCN-d_3, 25 °C. Atom numbering is shown in Scheme 1.

caused significant changes in the chemical shifts of most protons (Figures S9−S18, Supporting Information). When the bimolecular D−A complexes of (*E*)-**2** with (**3**−**5**)**a**,**b** are formed, some proton signals of the donor and the acceptor experience large upfield shifts (up to 0.9 ppm) resulting from the mutual shielding effect. The signals of most CH_2O groups of (*E*)-**2** show downfield shifts (up to 0.23 ppm) due to the electron-withdrawing effect of the NH_3^+ groups coordinated to the crown ether moieties of (*E*)-**2** *via* hydrogen bonds.

It has been previously shown that a high excess concentration of stilbene (*E*)-**1** (~0.01 M) in mixtures with acceptors (**3**−**5**)**a**,**b** can lead to the formation of termolecular D−A−D complexes in which the acceptor molecule is arranged in a stack between two molecules of the donor.[4,19] In MeCN, the stability constants of these complexes, $K_{2:1}$ = [D·A·D]/([D·A][D]), vary between $10^{1.7}$ and $10^{3.3}$ M^{-1} depending on the acceptor structure. Azobenzene (*E*)-**2** is also able to form D−A−D complexes with acceptors (**3**−**5**)**a**,**b**, as evidenced by an increase in the upfield shifts of the proton signals of the acceptor with an increase in the excess concentration of the donor (Figure 4c,d).

The stability constants for complexes of donors (*E*)-**1** and (*E*)-**2** with acceptors **3**−**5** and 1,10-diammoniodecane diperchlorate (**7**), as measured by ^{1}H NMR titration, are collected in Table 4. On the whole, the data on the relative stability of complexes (*E*)-**1**·(**3**−**5**)**a**,**b** and (*E*)-**2**·(**3**−**5**)**a**,**b** are in agreement with the corresponding data obtained by spectrophotometry and confirm the conclusion about weaker intermolecular charge-transfer interactions in the supramolecular complexes involving azobenzene (*E*)-**2**. Further evidence for this conclusion is the fact that the complexes of (*E*)-**2** with model acceptors (*E*)-**4c** and **5c** having no ammonium groups are less stable than the corresponding complexes of (*E*)-**1** ($\Delta\log K_{1:1}$ = 0.2−0.3; ^{1}H NMR data on the complexation of (*E*)-**2** with (*E*)-**4c** and **5c** are presented in Figures S19 and S20 in the Supporting Information).

The termolecular D−A−D complexes of (*E*)-**2** with the diammonium compounds having planar acceptor moieties, *viz.* (*E*)-**4a**,**b** and **5a**,**b**, are less stable than the corresponding complexes of (*E*)-**1** ($\Delta\log K_{2:1}$ = 0.2−0.5). The reverse situation is observed with nonplanar viologens **3a**,**b**. Presumably, this is due to the C−H···π-N=N contacts that occur between the viologen and azobenzene moieties in the sterically

https://dx.doi.org/10.1021/acsomega.0c03441
ACS Omega 2020, 5, 25993−26004

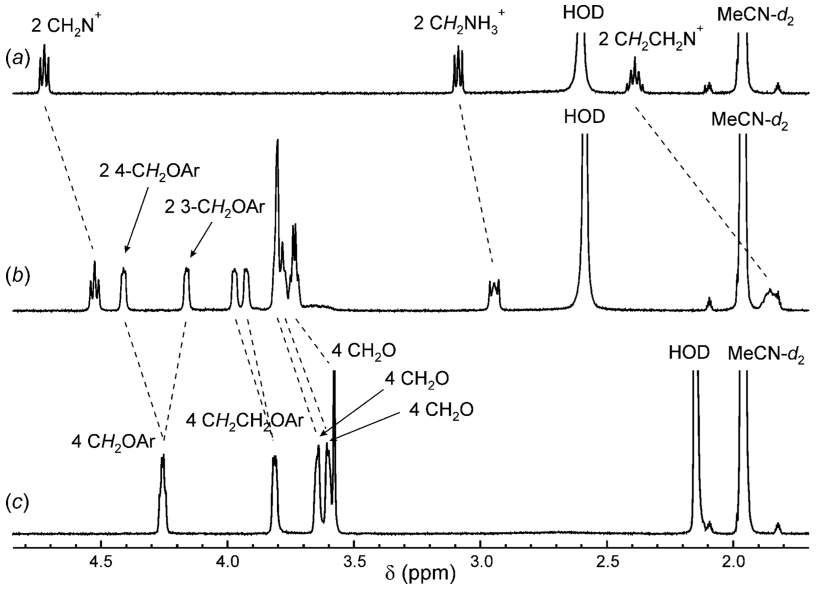

Figure 5. ^{1}H NMR spectra (aliphatic region) of (a) viologen **3b** (1 mM), (b) an equimolar mixture of viologen **3b** and azobenzene (*E*)-**2**, and (c) azobenzene (*E*)-**2** (1 mM); MeCN-d_3, 25 °C.

Table 4. Stability Constants for Complexes of Donors (*E*)-1 and (*E*)-2 with Acceptors 3−5 and Diammonium Compound 7, as Measured by ^{1}H NMR Titration[a]

	(*E*)-**1**		(*E*)-**2**	
compound	log $K_{1:1}$	log $K_{2:1}$	log $K_{1:1}$	log $K_{2:1}$
3a	6.8[b]	2.72[b]	6.9	2.92
3b	8.9[b]	1.79[b]	7.8	2.59
(*E*)-**4a**	9.0[b]	2.78[c]	8.4	2.27
(*E*)-**4b**	8.9[b]	3.27[c]	8.0	2.81
(*E*)-**4c**	1.14[c]		0.86	
5a	7.1[b]	3.22[b]	6.3	2.79
5b	9.3[b]	2.34[b]	7.8	2.04
5c	1.65[b]		1.45	
7	7.58[d]		7.34	

[a]In MeCN-d_3; 25 ± 1 °C; $K_{1:1}$ = [D·A]/([D][A]), M^{-1}; $K_{2:1}$ = [D·A·D]/([D·A][D]), M^{-1}. The stability constants are measured to within about ±30%. [b]From ref 4. [c]From ref 19. [d]Measured by spectrophotometry, ref 18.

unstrained D−A−D complexes, increasing the complex stability.

2.4. X-ray Diffraction Study. Azobenzene (*E*)-**2** like stilbene (*E*)-**1** can adopt two symmetrical conformations, *s-syn,s-syn* and *s-anti,s-anti*, associated with the rotation of the benzocrown moieties around the single bonds (Scheme 2). Stilbene (*E*)-**1** was reported to crystallize as an *s-anti,s-anti* conformer in the *C*2/*c* space group.[19] The X-ray analysis of crystalline azobenzene (*E*)-**2** showed that this compound despite its geometric similarity to stilbene (*E*)-**1** crystallizes in a different space group ($P2_1/c$) and exhibits a disorder with the *s-syn,s-syn* and *s-anti,s-anti* conformers situated in the same position with the site occupation ratio of 0.54:0.46 (Figure 6a). Since the conformers occupy a centrosymmetric position, their azobenzene moieties are perfectly planar. The bond lengths in the C(1)−N(1)═N(1A) fragment are 1.419(8) and 1.249(11) Å, and those in the C(1′)−N(1′)═N(1′A) fragment are 1.411(10) and 1.288(13) Å. The crown ether moieties of azobenzene (*E*)-**2** are also disordered.

Scheme 2. Single-Bond Conformers of Azobenzene (*E*)-2

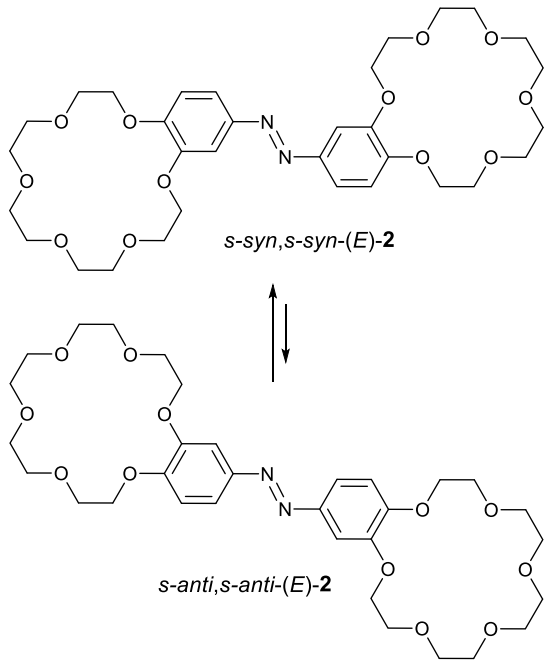

Figure 6b shows the main components in the crystalline complex with formula (*E*)-**2**·8$C_2H_7Br_2N$, formed by azobenzene (*E*)-**2** and 2-bromoethylammonium bromide (the latter compound was used in the synthesis of **3a**, (*E*)-**4a**, and **5a**).[4,19] The two bromoethylammonium cations in the presented structure are bound to the oxygen atoms of the 18-crown-6 ether moieties of (*E*)-**2**, mainly *via* bifurcated hydrogen bonds. The distances N(2)H···O(crown) vary between 2.01 and 2.34 Å, and the bond angles at the H atoms are 127−151°, which corresponds to moderate-strength hydrogen bonds. The distance between the nitrogen atoms of the bromoethylammonium ions coordinated with the crown ether moieties of (*E*)-**2** is 13.92 Å. The bis(crown)azobenzene has an *s-syn,s-syn* conformation with the bond lengths of 1.423(12) and

https://dx.doi.org/10.1021/acsomega.0c03441
ACS Omega 2020, 5, 25993−26004

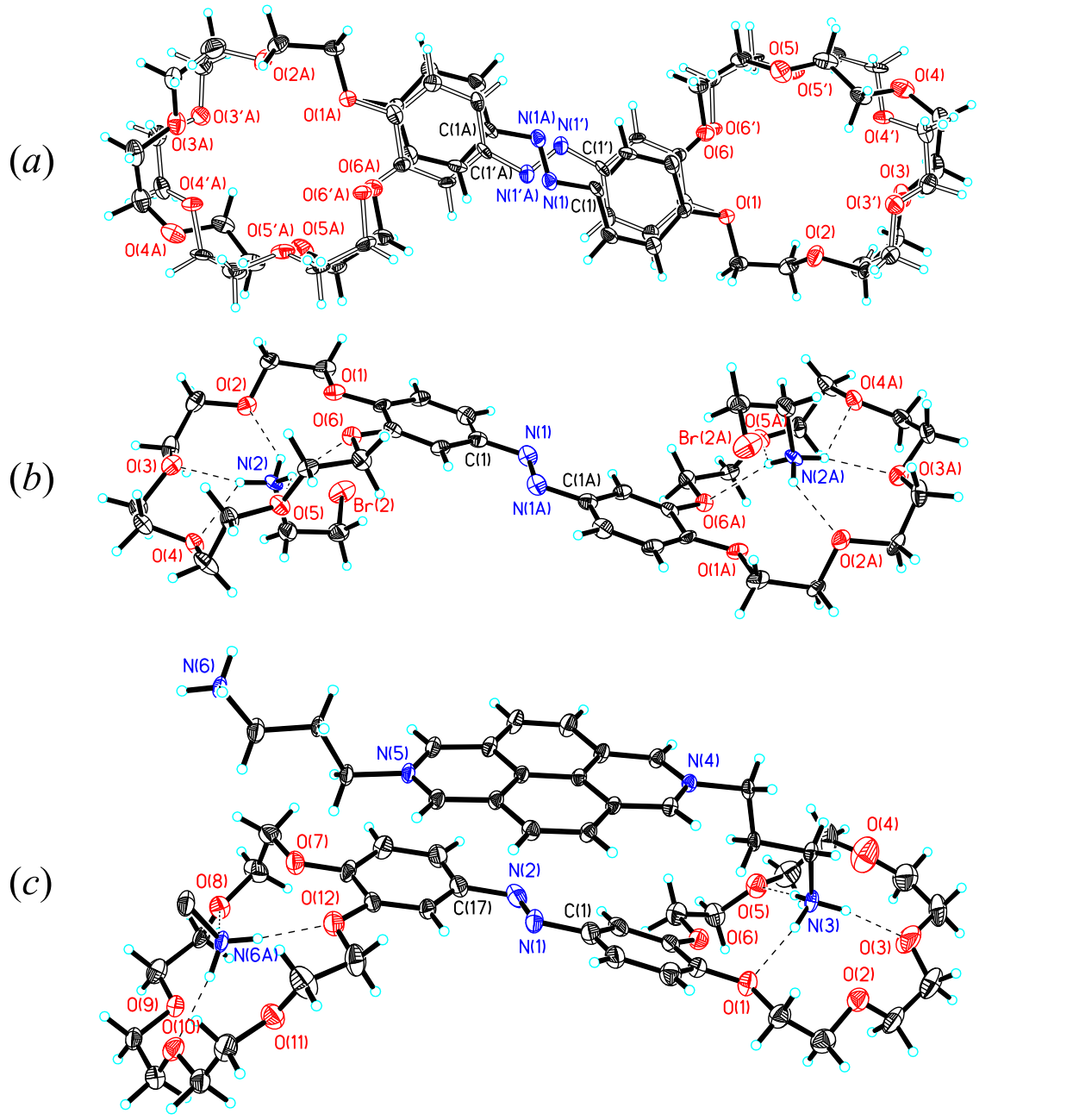

Figure 6. Structure (a) of crystalline azobenzene (*E*)-**2** (the bonds in the minor *s-anti,s-anti* conformer are depicted by hollow lines), (b) of the main components in crystalline complex (*E*)-**2**·8$C_2H_7Br_2N$, and (c) of the main components in crystalline complex [(*E*)-**2**·**5b**]·MeCN·0.5C_6H_6. Thermal ellipsoids are drawn at the 50% (a, b) or 30% (c) probability level; hydrogen bonds are shown with dashed lines, and symbols A are added to the atoms that belong to the symmetrically related sites.

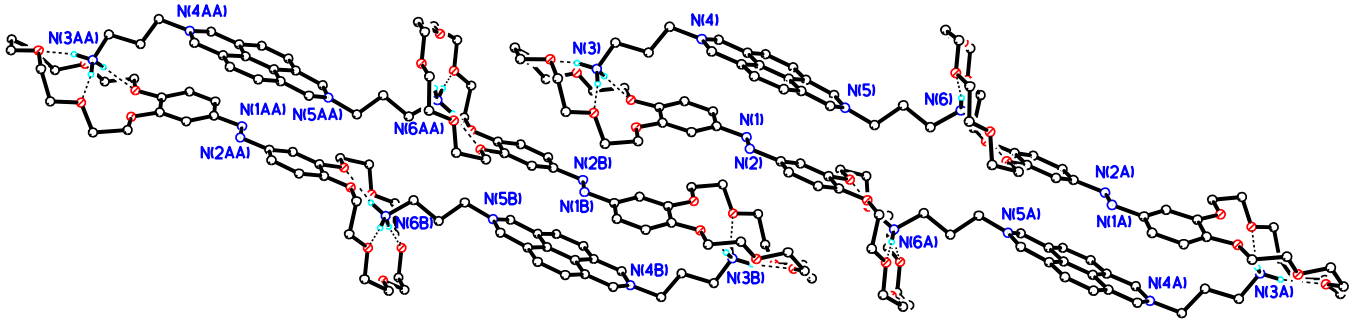

Figure 7. Packing of the main components in crystalline complex [(*E*)-**2**·**5b**]·MeCN·0.5C_6H_6.

https://dx.doi.org/10.1021/acsomega.0c03441
ACS Omega 2020, 5, 25993−26004

1.262(14) Å in the C(1)−N(1)═N(1A) fragment. The crystal unit cell of (*E*)-**2**·8$C_2H_7Br_2N$ includes three more independent bromoethylammonium cations that form multiple hydrogen bonds with bromide anions. Due to the centrosymmetric position of the bis(crown)azobenzene in the unit cell, its chromophoric moiety is perfectly planar.

The main components in the crystalline complex with formula [(*E*)-**2**·**5b**]·MeCN·0.5C_6H_6 are presented in Figure 6c. The molecules of azobenzene (*E*)-**2** and diazapyrene **5b** occupy general positions in the crystal unit cell and their chromophoric moieties are not perfectly planar: the dihedral angle between the planes of the benzene rings in (*E*)-**2** is 19.4° and that between the planes of the formally pyridine cycles in **5b** is 3.5°. The bond lengths in the C(1)−N(1)═N(2)−C(17) fragment of (*E*)-**2** are 1.430(7), 1.272(7), and 1.474(7) Å, respectively. The ammonium groups N(3)H_3^+ and N(6A)-H_3^+ form directional hydrogen bonds with the oxygen atoms of the crown ether moieties of (*E*)-**2**. The distances N(3)H···O(1,3,5) and N(6A)H···O(8,10,12) vary between 1.82 and 2.08 Å, and the bond angles at the H atoms are 170−175°. The distance between the N(3) and N(6A) atoms is 14.90 Å.

As can be seen from Figure 7, the crystalline structure of complex (*E*)-**2**·**5b** is different from the pseudocyclic bimolecular structure observed in solution (Scheme 1). In the single crystal, this complex is observed as a pseudocyclic tetramolecular structure composed of two molecules of azobenzene (*E*)-**2** and two tetracations of diazapyrene **5b**. There are two stacked pairs of molecules (*E*)-**2** and **5b** in the tetramolecular complex. The chromophoric moieties of (*E*)-**2** and **5b** in each pair are closely spaced and are largely projected onto each other. The mean planes of these moieties are nearly parallel to each other (the inclination angle between the planes is as low as 10.4°). All of this suggests significant π-stacking interactions between (*E*)-**2** and **5b** in the pseudocyclic tetramolecular complex. At the same time, there are no such interactions between neighboring tetramolecular complexes. Other packing patterns have been observed for crystalline complexes (*E*)-**1**·**3a**, (*E*)-**1**·**3b**, and (*E*)-**1**·(*E*)-**4a**[4,37] and for the crystalline complex of (*E*)-**2** with a bis(ammoniopropyl) derivative of (*E*)-1,2-di(3-pyridyl)ethylene.[38]

2.5. DFT and TD-DFT Calculations. The molecular structures of azobenzene (*E*)-**2** and its pseudocyclic complex with viologen **3b** in MeCN were calculated by DFT using the M06-2X functional and the solution model density (SMD) solvation model (Section 4.8). The electronic transition energies for (*E*)-**2** and (*E*)-**2**·**3b** were calculated by TD-DFT using the CAM-B3LYP functional (Section 4.8). The rationale for using the CAM-B3LYP functional in the TD-DFT calculations is given in the Supporting Information (details of TD-DFT calculations; Table S1 and Figure S2).

Figure 8 shows the most probable conformations of (*E*)-**2** and (*E*)-**2**·**3b** (detailed conformational analysis of (*E*)-**2** and (*E*)-**2**·**3b**, as well as (*E*)-**1** and (*E*)-**1**·**3b** will be published elsewhere). According to our calculations, the *s-syn,s-syn* conformation of compound (*E*)-**2** predominates in solution. The azobenzene moiety in (*E*)-**2** adopts almost planar conformation; the torsion angles between the N═N bond and the benzene rings are as low as 0.31 and −0.31° (C_i-symmetrical structure). The N═N and C−N bond lengths are 1.250 and 1.416 Å, respectively. The macrocyclic fragments of (*E*)-**2** have a crown-like conformation typical of benzo-18-crown-6 ethers. Such conformations are observed in the minor conformer of crystalline (*E*)-**2** and in the crystalline complexes

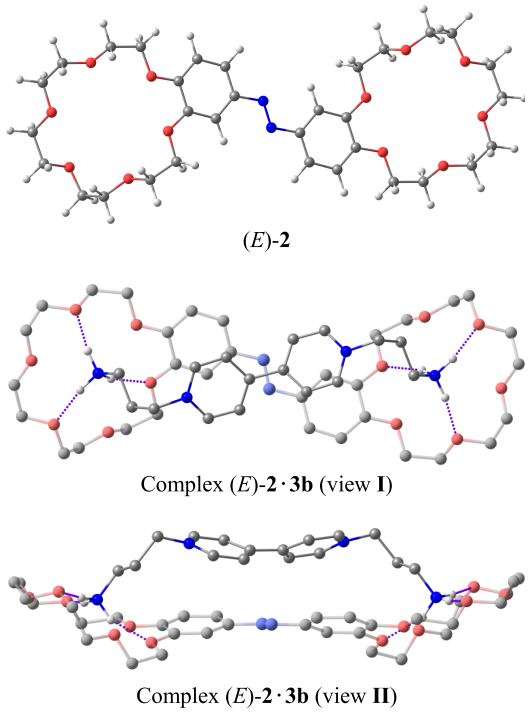

Figure 8. Most probable conformations of azobenzene (*E*)-**2** and complex (*E*)-**2**·**3b** in MeCN, according to DFT calculations; the complex is presented in two views, and the hydrogen atoms in the complex are not shown except those of the ammonium groups.

of (*E*)-**2** with 2-bromoethylammonium bromide and diammonium compound **5b** (Figure 6).

Complex (*E*)-**2**·**3b** was calculated in a C_2-symmetrical conformation. The azobenzene moiety in this complex is nonplanar; the torsion angles between the N═N bond and the benzene rings are 15.3°. The torsion angle between the pyridinium rings in viologen **3b** is 36.6°. The ammoniopropyl substituents in **3b** adopt a *trans,gauche* conformation. The distance between the center of the bond connecting the pyridinium rings and the center of the N═N bond of (*E*)-**2** is 3.06 Å.

The theoretical parameters of low-energy electronic transitions in (*E*)-**2** and (*E*)-**2**·**3b** are presented in Table 5. The transition energies calculated by TD-DFT were corrected by subtracting 0.127 eV; the justification for using this correction factor is given in the Supporting Information (details of TD-DFT calculations; Table S1 and Figure S2).

Table 5. Theoretical Parameters of Low-Energy Electronic Transitions in Azobenzene (*E*)-2 and Complex (*E*)-2·3b in MeCN

compound	transition	energy[a], eV (nm)	oscillator strength	λ_{max}[b], nm
(*E*)-**2**	S_0-S_1, $n\pi^*$	2.91 (426)	0	
	S_0-S_2, $\pi\pi^*$	3.28 (378)	1.31	378, 389
(*E*)-**2**·**3b**	S_0-S_1, $n\pi^*$ (**2**)	2.81 (441)	0.11	
	S_0-S_2, CT (**2** → **3b**)	2.99 (414)	0.0004	
	S_0-S_3, $\pi\pi^*$ (**2**)	3.40 (365)	0.94	371

[a]The transition energies calculated by time-dependent DFT were corrected by subtracting 0.127 eV. [b]λ_{max} is the position of the long-wavelength absorption maximum in the observed UV−vis spectrum (Figure 1).

https://dx.doi.org/10.1021/acsomega.0c03441
ACS Omega 2020, 5, 25993−26004

The TD-DFT calculations predict an increase in the energy and a decrease in the oscillator strength of the azobenzene $\pi\pi^*$ transition upon the complexation of (*E*)-**2** with **3b**, which is in agreement with the UV−vis spectroscopy data (Figure 1). The calculations also predict that the formation of complex (*E*)-**2**·**3b** should lead to a decrease in the energy and an increase in the oscillator strength of the azobenzene $n\pi^*$ transition, as well as to the appearance of a CT transition (azobenzene-to-viologen) in the region between the azobenzene $\pi\pi^*$ and $n\pi^*$ transitions. These data indicate that the absorption rise at the long-wavelength edge of the UV−vis spectrum of (*E*)-**2**, observed upon the formation of complex (*E*)-**2**·**3b** (Figure 1), is mostly due to the changes in the characteristics of the azobenzene $n\pi^*$ transition. The absorption band associated with the CT transition in (*E*)-**2**·**3b** is indiscernible in the experimental spectrum because it has a very low intensity and is overlapped with the broad and more intense bands associated with the azobenzene $\pi\pi^*$ and $n\pi^*$ transitions.

3. CONCLUSIONS

The highly stable bimolecular D−A complexes of bis(crown)-azobenzene (*E*)-**2** with acceptor molecules (**3**−**5**)**a**,**b** have a pseudocyclic structure due to ditopic coordination of the ammonium groups of the acceptor to the crown ether moieties of the donor. The azobenzene complexes are characterized by a somewhat lower stability in comparison with the corresponding complexes of stilbene (*E*)-**1** (strong π-donor), which is attributable mostly to weaker CT interactions due to the lower electron-donating ability of (*E*)-**2**. The low-energy CT transition in the D−A complex of (*E*)-**2** with viologen derivative **3b** lies between the local $\pi\pi^*$ and $n\pi^*$ transitions of the azobenzene and is characterized by a very low oscillator strength. The absorption band associated with the CT transition is unobservable since it is overlapped with the broad and more intense $\pi\pi^*$ and $n\pi^*$ bands. The complexation of (*E*)-**2** with **3b** leads to a decrease in the $E \rightarrow Z$ photoisomerization quantum yield of (*E*)-**2** almost by an order of magnitude, which probably arises from the intermolecular electron transfer that occurs in the $^1\pi\pi^*$ excited state of the azobenzene and competes with the $^1\pi\pi^* \rightarrow {}^1n\pi^*$ internal conversion.

The results of this study can be used for the targeted design of new types of photoactive supramolecular systems stabilized *via* the formation of numerous hydrogen bonds, in particular, for the development of optical molecular sensors for acceptor compounds.

4. EXPERIMENTAL SECTION

4.1. Materials. Bis(18-crown-6)stilbene (*E*)-**1**,[39] bis(18-crown-6)azobenzene (*E*)-**2**,[40] bis(ammonioalkyl)-containing acceptor compounds **3a**,**b**,[4] (*E*)-**4a**,**b**,[19,41] and **5a**,**b**,[4] and model acceptor compounds (*E*)-**4c**[41] and **5c**[42] were synthesized by known procedures. 1,9-Diammoniononane diperchlorate (**6**) and 1,10-diammoniodecane diperchlorate (**7**) were prepared as described previously.[38,43] 2-Bromoethylammonium bromide (Sigma-Aldrich) and MeCN (special purity grade, water content <0.03%, v/v, Cryochrom) were used as received.

4.1.1. Synthesis of Complexes of (E)-2 with Compounds (3−5)a,b and 7 in the Solid State (General Method). A mixture of bis-crown azobenzene (*E*)-**2** (13 mg, 20 μmol) and a bis-ammonium compound [(**3**−**5**)**a**,**b** or **7**, 20 μmol] was dissolved in MeCN (~5 mL). If necessary, a few drops of water were added to achieve complete dissolution of the mixture. The solution was slowly (for 1−2 weeks) saturated with benzene or a mixture of benzene and dioxane (~2:1, v/v) by the vapor diffusion method at room temperature in the dark. The precipitate thus formed was decanted and dried *in vacuo* to give a complex between (*E*)-**2** and (**3**−**5**)**a**,**b** (or between (*E*)-**2** and **7**) as a fine-crystalline or amorphous powder. The complexes were obtained in yields of >70%. The formal 1:1 composition of complexes was proved by ^{1}H NMR in DMSO-d_6 (Figures S3−S8, Supporting Information). In this solvent, the complexes decomposed to give a mixture of free components.

Complex (*E*)-**2**·**3a**, dark-orange powder, mp 264−266 °C dec. IR, ν/cm^{-1}: 3164 (N^+−H). Calcd for $C_{32}H_{46}N_2O_{12}$·$C_{14}H_{22}Cl_4N_4O_{16}$·2.5$H_2O$ (1339.90): C, 41.23; H, 5.49; N, 6.27; found: C, 41.17; H, 5.18; N, 6.14%.

Complex (*E*)-**2**·**3b**, dark-orange powder, mp 189−191 °C. IR, ν/cm^{-1}: 3188 (N^+−H). Calcd for $C_{32}H_{46}N_2O_{12}$·$C_{16}H_{26}Cl_4N_4O_{16}$·0.5$C_6H_6$·1.5$H_2O$ (1389.00): C, 44.10; H, 5.66; N, 6.05; found: C, 43.93; H, 5.49; N, 6.02%.

Complex (*E*)-**2**·(*E*)-**4a**, red-orange crystals, mp 262−265 °C dec. IR, ν/cm^{-1}: 3177 (N^+−H). Calcd for $C_{32}H_{46}N_2O_{12}$·$C_{16}H_{24}Cl_4N_4O_{16}$·0.5$C_6H_6$·$H_2O$ (1377.97): C, 44.45; H, 5.49; N, 6.10; found: C, 44.58; H, 5.56; N, 5.71%.

Complex (*E*)-**2**·(*E*)-**4b**, red-orange crystals, mp 230−233 °C dec. IR, ν/cm^{-1}: 3198 (N^+−H). Calcd for $C_{32}H_{46}N_2O_{12}$·$C_{18}H_{28}Cl_4N_4O_{16}$ (1348.96): C, 44.52; H, 5.53; N, 6.23; found: C, 44.46; H, 5.54; N, 6.08%.

Complex (*E*)-**2**·**5a**, dark-orange powder, mp 235−236 °C dec. IR, ν/cm^{-1}: 3178 (N^+−H). Calcd for $C_{32}H_{46}N_2O_{12}$·$C_{18}H_{22}Cl_4N_4O_{16}$·0.5$C_6H_6$·2.5$H_2O$ (1427.00): C, 44.61; H, 5.37; N, 5.89; found: C, 44.56; H, 5.40; N, 5.64%.

Complex (*E*)-**2**·**5b**, dark-orange powder, mp > 250 °C dec. IR, ν/cm^{-1}: 3191 (N^+−H). Calcd for $C_{32}H_{46}N_2O_{12}$·$C_{20}H_{26}Cl_4N_4O_{16}$ (1370.96): C, 45.56; H, 5.29; N, 6.13; found: C, 45.74; H, 5.21; N, 6.11%.

Complex (*E*)-**2**·**7**, yellow-orange powder, mp 160−165 °C. IR, ν/cm^{-1}: 3190 (N^+−H). Calcd for $C_{32}H_{46}N_2O_{12}$·$C_{10}H_{26}Cl_2N_2O_8$ (1023.95): C, 49.27; H, 7.09; N, 5.47; found: C, 49.17; H, 7.07; N, 5.39%.

4.2. Methods. Melting points (uncorrected) were measured in capillaries on a Mel-Temp II apparatus. ^{1}H NMR spectra were recorded on a Bruker DRX500 instrument in DMSO-d_6 and MeCN-d_3 using the signal from the solvent as the internal standard (δ_H 2.50 and 1.96, respectively). IR spectra were measured on a Bruker IFS-113V spectrometer in Nujol between KBr plates. UV−vis absorption spectra were recorded on a Specord M40 spectrophotometer in quartz cells with ground-in stoppers. All manipulations with solutions of azobenzene (*E*)-**2** and its complexes were carried out in a dark room under red light (daylight induces the *E*−*Z* photoisomerization). Stationary photolysis was performed using glass-filtered light of a high-pressure Hg lamp (λ = 365, 405, or 436 nm); the light intensity was measured by chemical actinometry. Elemental analyses were carried out at the Microanalytical Laboratory of the A.N. Nesmeyanov Institute of Organoelement Compounds (Moscow, Russian Federation); the samples for elemental analysis were dried *in vacuo* at 80 °C. Compounds **3**−**7** and their complexes containing perchlorate anions are nonexplosive.

4.3. Cyclic Voltammetry. Cyclic voltammetry experiments were carried out using a three-electrode system. A glassy

https://dx.doi.org/10.1021/acsomega.0c03441
ACS Omega 2020, 5, 25993−26004

carbon disk (d = 1.8 mm) was used as the working electrode. The reference electrode was Ag|AgCl|KCl (aq, sat.). A platinum plate (S = 0.5 cm^2) served as the auxiliary electrode. Cyclic voltammograms were measured in MeCN solutions in the presence of Bu_4NClO_4 (0.1 M) at 22 °C. All solutions were deaerated by argon purging. The potential scanning rate was 200 mV s^{-1}. Ferrocene (1 mM) was used as the internal reference. The concentrations of reactants were 1 mM.

4.4. Spectrophotometric Titration (SPT). SPT experiments were conducted in MeCN in 1 cm and 5 cm cells. The stability constants and absorption spectra of complexes were determined by globally fitting the SPT data to an appropriate complexation model.[44]

The stability constant of the 1:1 complex of azobenzene (*E*)-**2** with 1,9-diammoniononane perchlorate (**6**) was measured by direct SPT: the total concentration of (*E*)-**2** was maintained constant at 4×10^{-6} M (5 cm cell), and the total concentration of **6** varied incrementally from 0 to 2×10^{-5} M.

The stability constants of the bimolecular D−A complexes of (*E*)-**2** with acceptor compounds (**3**−**5**)**a**,**b** were measured using competitive SPT: the total concentrations of the donor, (*E*)-**2**, and the acceptor were maintained constant at 2×10^{-5} M (1 cm cell), and the total concentration of the competing donor, (*E*)-**1**, varied incrementally from 0 to 1×10^{-4} M. The known stability constants of complexes (*E*)-**1**•(**3**−**5**)**a**,**b**[4] were used as nonvariable parameters in the global fitting of the SPT data.

4.5. *E*−*Z* Photoisomerization Quantum Yields. The quantum yields for the forward and back *E*−*Z* photoisomerization reactions (φ_{E-Z} and φ_{Z-E}) of azobenzene (*E*)-**2** in the free and complexed forms were determined from the kinetics of UV−vis absorption spectra observed upon the steady-state irradiation of MeCN solutions with 365 nm light. The absorption spectrum of the pure *Z*-isomer was calculated using the spectra of the *E*−*Z* photostationary states attained upon irradiation at different wavelengths (365, 405, and 436 nm) on the assumption that the $\varphi_{E-Z}/\varphi_{Z-E}$ ratio is independent of the irradiation wavelength. The spectroscopic data were treated using global analysis methods, as described previously.[45] The photoisomerization quantum yields are measured to within ±20%.

4.6. ^{1}H NMR Titration. Experiments were conducted in MeCN-d_3 solutions at 25 ± 1 °C. The stability constants for the termolecular D−A−D complexes ($K_{2:1}$, M^{-1}) of donor (*E*)-**2** with acceptors (**3**−**5**)**a**,**b**, as well as for the bimolecular D−A complexes ($K_{1:1}$, M^{-1}) of (*E*)-**2** with model acceptors (*E*)-**4c** and **5c**, were determined by analyzing the shifts of the proton signals of the acceptor ($\Delta\delta_H$) as a function of the concentration of the added donor.[4] The total concentration of the acceptor was maintained constant at ∼1 mM, and the total concentration of the donor varied from 0 to 10−20 mM.

The stability constants for the bimolecular D−A complexes of (*E*)-**2** with acceptors (**3**−**5**)**a**,**b** were measured using competitive titration:[4] the total concentrations of the donor and the acceptor were maintained constant at ∼1.2 and ∼1.0 mM, respectively, and the total concentration of the competing reactant, 1,10-diammoniodecane diperchlorate (**7**), varied from 0 to 10 mM.

The titration data were treated using the HYPNMR program.[46]

4.7. X-ray Diffraction Analysis. Single crystals of azobenzene (*E*)-**2** were obtained by slow evaporation of a CH_2Cl_2−hexane solution (∼1:1, v/v) in the dark. Single crystals of complexes (*E*)-**2**·8$C_2H_7Br_2N$ and [(*E*)-**2**•**5b**]·MeCN·0.5C_6H_6 were grown as follows: a mixture of (*E*)-**2** with 2-bromoethylammonium bromide or compound **5b** was dissolved in MeCN, and then the solution was slowly saturated with benzene by the vapor diffusion method at an ambient temperature in the dark.

A selected single crystal was coated with perfluorinated oil and mounted on a Bruker SMART Apex-II CCD diffractometer [graphite monochromatized Mo Kα radiation (λ = 0.71073 Å), ω scan mode] under a stream of cooled nitrogen [T = 120(2) K] to measure crystallographic parameters and intensities of experimental reflections. Data reduction was performed using the SAINT program.[47]

The structures were solved by direct methods and refined by least squares against F^2 with anisotropic thermal parameters for all nonhydrogen atoms using the SHELXL software.[48] The hydrogen atoms were fixed at calculated positions at carbon and nitrogen atoms and then refined using a riding model.

Crystal data for (*E*)-**2**: $C_{32}H_{46}N_2O_{12}$, M = 650.71, monoclinic, space group $P2_1/c$ (no. 14), yellow plate, a = 20.838(5) Å, b = 9.193(2) Å, c = 8.4373(19) Å, β = 95.134(5)°, V = 1609.7(6) Å^3, T = 120(2) K, Z = 2, μ = 0.103 mm^{-1}, ρ_{calc} = 1.342 g cm^{-3}, $2\theta_{max}$ = 56.00°, 8982 reflections measured, 3827 unique (R_{int} = 0.0450), R_1 = 0.0885 (2591 reflections with $I > 2\sigma(I)$), wR_2 = 0.2240 (all data), goodness-on-fit on F^2 = 1.037, 356 parameters, min/max residual electron density = −0.24/0.36 $\bar{e}$ Å^{-3}. AFIX 66, SADI, and ISOR commands were applied for the disordered moieties to constrain their geometry and anisotropic thermal parameters.

Crystal data for (*E*)-**2**·8$C_2H_7Br_2N$: $C_{48}H_{102}Br_{16}N_{10}O_{12}$, M = 2289.95, monoclinic, space group $P2_1/n$ (no. 14), yellow plate, a = 16.5989(6) Å, b = 8.1632(3) Å, c = 28.6162(11) Å, β = 92.816(4)°, V = 3872.8(2) Å^3, T = 120(2) K, Z = 2, μ = 8.325 mm^{-1}, ρ_{calc} = 1.964 g cm^{-3}, $2\theta_{max}$ = 58.00°, 39 713 reflections measured, 10 295 unique (R_{int} = 0.1241), R_1 = 0.0823 (6518 reflections with $I > 2\sigma(I)$), wR_2 = 0.2111 (all data), goodness-on-fit on F^2 = 1.039, 450 parameters, min/max residual electron density = −2.65/2.12 $\bar{e}$ Å^{-3}. Ion Br(5)CH_2CH_2N(5)H_3^+ is disordered over two positions with an occupancy ratio of 0.61:0.39. Atom Br(3) in Br(3)CH_2CH_2N(3)H_3^+ ion is disordered over two positions with an occupancy ratio of 0.93:0.07. Anion Br(8) is disordered over two positions with an occupancy ratio of 0.60:0.40. The very high absorption and thin-plate shape of the crystal resulted in a decrease in the accuracy of this X-ray diffraction experiment. ISOR command was applied to constrain the anisotropic thermal parameters of some atoms of the disordered moieties.

Crystal data for [(*E*)-**2**•**5b**]·MeCN·0.5C_6H_6: $C_{57}H_{78}Cl_4N_7O_{28}$, M = 1451.06, triclinic, space group $P\bar{1}$ (no. 2), orange block, a = 12.5838(3) Å, b = 16.0616(4) Å, c = 17.8292(5) Å, α = 71.082(1)°, β = 79.353(1)°, γ = 80.748(1)°, V = 3330.45(15) Å^3, T = 120(2) K, Z = 2, μ = 0.268 mm^{-1}, ρ_{calc} = 1.447 g cm^{-3}, $2\theta_{max}$ = 58.00°, 31 347 reflections measured, 17424 unique (R_{int} = 0.0424), R_1 = 0.1119 (8683 reflections with $I > 2\sigma(I)$), wR_2 = 0.3653 (all data), goodness-on-fit on F^2 = 1.139, 923 parameters, min/max residual electron density = −0.74/1.80 $\bar{e}$ Å^{-3}. The benzene molecule of solvation is situated at a symmetry center and disordered over two positions with an occupancy ratio of 0.62:0.38. One of the four perchlorate anions is strongly disordered over two rotationally related positions with an occupancy ratio of 0.62:0.38. This disorder reduces the

https://dx.doi.org/10.1021/acsomega.0c03441
ACS Omega 2020, 5, 25993−26004

accuracy of the X-ray diffraction experiment. SADI and ISOR commands were used in the refinement process.

The crystallographic data for (*E*)-**2**, (*E*)-**2**·8$C_2H_7Br_2N$, and [(*E*)-**2**·**5b**]·MeCN·0.5C_6H_6 were deposited with the Cambridge Crystallographic Data Centre under numbers CCDC 1985189, 1985190, and 1985191, respectively.

4.8. Computational Details. DFT calculations were performed using the Gaussian 16 program package.[49] Geometry optimizations were carried out with the M06-2X functional[50] and the 6-31G(d) basis set.[51,52] To accelerate the calculations, the two-electron integral accuracy was set to 10^{-10} (the default value is 10^{-12}). The default optimization criteria were tightened by six times using the internal option IOp(1/7 = 50). The universal solvation model called solution model density (SMD)[53] was employed to simulate the effects of MeCN as the experimental solvent. All geometry optimizations were followed by frequency calculations to verify the nature of stationary points and to compute thermochemical quantities. The thermochemical analysis was carried out using a scale factor of 0.9678 for harmonic frequencies.[54] The Gibbs free energy in solution (G_{soln}) was calculated by the formula

$$G_{soln} = E_{soln} + \Delta G_{corr}$$

where E_{soln} is the electronic energy in solution, and ΔG_{corr} is the thermal correction to the free energy, including the zero-point vibrational energy. The ΔG_{corr} values were calculated at the same level of theory as that used for geometry optimizations, whereas the E_{soln} values were derived from the single-point M06-2X calculations with the 6-311G(2df,2p) basis set;[55,56] the large basis set was used to minimize basis set superposition errors for complexes.

TD-DFT calculations were carried out on the M06-2X/6-31G(d)/SMD geometries using the CAM-B3LYP functional,[57] the 6-311G(2d,p) basis set,[55,58] and the SMD solvation model.

■ ASSOCIATED CONTENT

Supporting Information

The Supporting Information is available free of charge at https://pubs.acs.org/doi/10.1021/acsomega.0c03441.

Cyclic voltammograms (Figure S1); details of TD-DFT calculations (Table S1 and Figure S2); ^{1}H NMR spectra (Figures S3−S20); and crystallographic information (Tables S2−S9) (PDF)

Crystallographic data (CIF)

Crystallographic data (CIF)

Crystallographic data (CIF)

Cartesian coordinates for DFT-calculated structures (XYZ)

Cartesian coordinates for DFT-calculated structures (XYZ)

Cartesian coordinates for DFT-calculated structures (XYZ)

Cartesian coordinates for DFT-calculated structures (XYZ)

Cartesian coordinates for DFT-calculated structures (XYZ)

■ AUTHOR INFORMATION

Corresponding Authors

Evgeny N. Ushakov − *Institute of Problems of Chemical Physics, Russian Academy of Sciences 142432, Russian Federation; Photochemistry Center of RAS, FSRC "Crystallography and Photonics", Russian Academy of Sciences, Moscow 119421, Russian Federation;* orcid.org/0000-0002-9969-5185; Email: e.n.ushakov@gmail.com

Sergey P. Gromov − *Photochemistry Center of RAS, FSRC "Crystallography and Photonics", Russian Academy of Sciences, Moscow 119421, Russian Federation; Department of Chemistry, M.V. Lomonosov Moscow State University, Moscow 119991, Russian Federation*; Email: spgromov@mail.ru

Authors

Timofey P. Martyanov − *Institute of Problems of Chemical Physics, Russian Academy of Sciences 142432, Russian Federation; Photochemistry Center of RAS, FSRC "Crystallography and Photonics", Russian Academy of Sciences, Moscow 119421, Russian Federation*

Artem I. Vedernikov − *Photochemistry Center of RAS, FSRC "Crystallography and Photonics", Russian Academy of Sciences, Moscow 119421, Russian Federation*

Asya A. Efremova − *Photochemistry Center of RAS, FSRC "Crystallography and Photonics", Russian Academy of Sciences, Moscow 119421, Russian Federation*

Anna A. Moiseeva − *Department of Chemistry, M.V. Lomonosov Moscow State University, Moscow 119991, Russian Federation*

Lyudmila G. Kuz'mina − *N.S. Kurnakov Institute of General and Inorganic Chemistry, Russian Academy of Sciences, Moscow 119991, Russian Federation*

Svetlana N. Dmitrieva − *Photochemistry Center of RAS, FSRC "Crystallography and Photonics", Russian Academy of Sciences, Moscow 119421, Russian Federation*

Judith A. K. Howard − *Department of Chemistry, Durham University, Durham DH1 3LE, United Kingdom*

Complete contact information is available at: https://pubs.acs.org/10.1021/acsomega.0c03441

Notes

The authors declare no competing financial interest.

■ ACKNOWLEDGMENTS

This work was supported by the Russian Science Foundation with respect to the electrochemical, photochemical, and NMR studies (Project No. 19-13-00020) and by the Ministry of Science and Higher Education of the Russian Federation with respect to the DFT calculations (State Assignment No. AAAA-A19-119070790003-7) and the synthesis of donor−acceptor complexes (State Assignment FSRC "Crystallography and Photonics" of RAS). L.G.K. thanks the Royal Society of Chemistry for an International Author grant (with respect to the X-ray diffraction study).

■ REFERENCES

(1) Günes, S.; Neugebauer, H.; Sariciftci, N. S. Conjugated polymer-based organic solar cells. *Chem. Rev.* **2007**, *107*, 1324−1338.

(2) Mori, T. Organic charge-transfer salts and the component molecules in organic transistors. *Chem. Lett.* **2011**, *40*, 428−434.

(3) Horiuchi, S.; Hasegawa, T.; Tokura, Y. Molecular donor−acceptor compounds as prospective organic electronics materials. *J. Phys. Soc. Jpn.* **2006**, *75*, No. 051016.

(4) Vedernikov, A. I.; Ushakov, E. N.; Efremova, A. A.; Kuz'mina, L. G.; Moiseeva, A. A.; Lobova, N. A.; Churakov, A. V.; Strelenko, Y. A.; Alfimov, M. V.; Howard, J. A. K.; Gromov, S. P. Synthesis, structure, and properties of supramolecular charge-transfer complexes between bis(18-crown-6)stilbene and ammonioalkyl derivatives of 4,4′-bipyridine and 2,7-diazapyrene. *J. Org. Chem.* **2011**, *76*, 6768−6779.

(5) Ushakov, E. N.; Nadtochenko, V. A.; Gromov, S. P.; Vedernikov, A. I.; Lobova, N. A.; Alfimov, M. V.; Gostev, F. E.; Petrukhin, A. N.; Sarkisov, O. M. Ultrafast excited state dynamics of the bi- and termolecular stilbene−viologen charge-transfer complexes assembled *via* host−guest interactions. *Chem. Phys.* **2004**, *298*, 251−261.
(6) Ke, X.-S.; Kim, T.; Lynch, V. M.; Kim, D.; Sessler, J. L. Flattened calixarene-like cyclic BODIPY array: a new photosynthetic antenna model. *J. Am. Chem. Soc.* **2017**, *139*, 13950−13956.
(7) Bill, N. L.; Ishida, M.; Kawashima, Y.; Ohkubo, K.; Sung, Y. M.; Lynch, V. M.; Lim, J. M.; Kim, D.; Sessler, J. L.; Fukuzumi, S. Long-lived charge-separated states produced in supramolecular complexes between anionic and cationic porphyrins. *Chem. Sci.* **2014**, *5*, 3888−3896.
(8) Sakai, H.; Ohkubo, K.; Fukuzumi, S.; Hasobe, T. Photoinduced processes of supramolecular nanoarrays composed of porphyrin and benzo[*ghi*]perylenetriimide units through triple hydrogen bonds with one-dimensional columnar phases. *Chem. - Asian J.* **2016**, *11*, 613−624.
(9) Shifrin, S. Charge-transfer complexes in biological systems. *Ann. N.Y. Acad. Sci.* **1969**, *158*, 148−160.
(10) Slifkin, M. A. *Charge Transfer Interactions of Biomolecules*; Academic Press: London, New York, 1971.
(11) Gutmann, F.; Johnson, C.; Keyzer, H.; Molnar, J. *Charge Transfer Complexes in Biological Systems*; Marcel Dekker: New York, 1997.
(12) Sjulstok, E.; Olsen, J. M. H.; Solov'yov, I. A. Quantifying electron transfer reactions in biological systems: what interactions play the major role? *Sci. Rep.* **2015**, *5*, No. 18446.
(13) Weber, S. Light-driven enzymatic catalysis of DNA repair: a review of recent biophysical studies on photolyase. *Biochim. Biophys. Acta, Bioenerg.* **2005**, *1707*, 1−23.
(14) Ritz, T. Quantum effects in biology: bird navigation. *Procedia Chem.* **2011**, *3*, 262−275.
(15) Roy, D. K.; Saha, A.; Mukherjee, A. K. Spectroscopic and thermodynamic study of charge transfer complexes of cloxacillin sodium in aqueous ethanol medium. *Spectrochim. Acta, Part A* **2005**, *61*, 2017−2022.
(16) Dozal, A.; Keyzer, H.; Kim, H. K.; Wang, W. W. Charge transfer complexes of K vitamins with several classes of antimicrobials. *Int. J. Antimicrob. Agents* **2000**, *14*, 261−265.
(17) Liao, L. B.; Zhou, H. Y.; Xiao, X. M. Spectroscopic and viscosity study of doxorubicin interaction with DNA. *J. Mol. Struct.* **2005**, *749*, 108−113.
(18) Ushakov, E. N.; Gromov, S. P.; Vedernikov, A. I.; Malysheva, E. V.; Botsmanova, A. A.; Alfimov, M. V.; Eliasson, B.; Edlund, U. G.; Whitesell, J. K.; Fox, M. A. Self-organization of highly stable electron donor−acceptor complexes *via* host−guest interactions. *J. Phys. Chem. A* **2002**, *106*, 2020−2023.
(19) Gromov, S. P.; Vedernikov, A. I.; Ushakov, E. N.; Lobova, N. A.; Botsmanova, A. A.; Basok, S. S.; Kuz'mina, L. G.; Churakov, A. V.; Strelenko, Y. A.; Alfimov, M. V.; Ivanov, E. I.; Howard, J. A. K.; Johnels, D.; Edlund, U. G. Novel supramolecular charge-transfer systems based on bis(18-crown-6)stilbene and viologen analogues bearing two ammonioalkyl groups. *New J. Chem.* **2005**, *29*, 881−894.
(20) Klajn, R. Immobilized azobenzenes for the construction of photoresponsive materials. *Pure Appl. Chem.* **2010**, *82*, 2247−2279.
(21) Merino, E.; Ribagorda, M. Control over molecular motion using the *cis*−*trans* photoisomerization of the azo group. *Beilstein J. Org. Chem.* **2012**, *8*, 1071−1090.
(22) Gelebart, A. H.; Mulder, D. J.; Varga, M.; Konya, A.; Vantomme, G.; Meijer, E. W.; Selinger, R. L. B.; Broer, D. J. Making waves in a photoactive polymer film. *Nature* **2017**, *546*, 632−636.
(23) Tabor, R. F.; McCoy, T. M.; Hu, Y.; Wilkinson, B. L. Physicochemical and biological characterisation of azobenzene-containing photoswitchable surfactants. *Bull. Chem. Soc. Jpn.* **2018**, *91*, 932−939.
(24) Dong, L.; Feng, Y.; Wang, L.; Feng, W. Azobenzene-based solar thermal fuels: design, properties, and applications. *Chem. Soc. Rev.* **2018**, *47*, 7339−7368.
(25) Li, S.; Wang, H.; Fang, J.; Liu, Q.; Wang, J.; Guo, S. Photo-isomerization energy storage using azobenzene and nanoscale templates: a topical review. *J. Therm. Sci.* **2020**, *29*, 280−297.
(26) Huang, X.; Li, T. Recent progress in the development of molecular-scale electronics based on photoswitchable molecules. *J. Mater. Chem. C* **2020**, *8*, 821−848.
(27) Velema, W. A.; Szymanski, W.; Feringa, B. L. Photopharmacology: beyond proof of principle. *J. Am. Chem. Soc.* **2014**, *136*, 2178−2191.
(28) Lerch, M. M.; Hansen, M. J.; van Dam, G. M.; Szymanski, W.; Feringa, B. L. Emerging targets in photopharmacology. *Angew. Chem., Int. Ed.* **2016**, *55*, 10978−10999.
(29) Agnetta, L.; Kauk, M.; Canizal, M. C. A.; Messerer, R.; Holzgrabe, U.; Hoffmann, C.; Decker, M. A. Photoswitchable dualsteric ligand controlling receptor efficacy. *Angew. Chem., Int. Ed.* **2017**, *56*, 7282−7287.
(30) Hauwert, N. J.; Mocking, T. A. M.; Da Costa Pereira, D.; Kooistra, A. J.; Wijnen, L. M.; Vreeker, G. C. M.; Verweij, E. W. E.; De Boer, A. H.; Smit, M. J.; De Graaf, C.; Vischer, H. F.; de Esch, I. J. P.; Wijtmans, M.; Leurs, R. Synthesis and characterization of a bidirectional photoswitchable antagonist toolbox for real-time GPCR photopharmacology. *J. Am. Chem. Soc.* **2018**, *140*, 4232−4243.
(31) Mehta, Z. B.; Johnston, N. R.; Nguyen-Tu, M.-S.; Broichhagen, J.; Schultz, P.; Larner, D. P.; Leclerc, I.; Trauner, D.; Rutter, G. A.; Hodson, D. J. Remote control of glucose homeostasis *in vivo* using photopharmacology. *Sci. Rep.* **2017**, *7*, No. 291.
(32) Wegener, M.; Hansen, M. J.; Driessen, A. J. M.; Szymanski, W.; Feringa, B. L. Photocontrol of antibacterial activity: shifting from UV to red light activation. *J. Am. Chem. Soc.* **2017**, *139*, 17979−17986.
(33) Butin, K. P.; Moiseeva, A. A.; Gromov, S. P.; Vedernikov, A. I.; Botsmanova, A. A.; Ushakov, E. N.; Alfimov, M. V. Prospects of electroanalytical investigations of supramolecular complexes of a bis-crown stilbene with viologen-like compounds bearing two ammonioalkyl groups. *J. Electroanal. Chem.* **2003**, *547*, 93−102.
(34) Fujino, T.; Arzhantsev, S. Yu.; Tahara, T. Femtosecond time-resolved fluorescence study of photoisomerization of *trans*-azobenzene. *J. Phys. Chem. A* **2001**, *105*, 8123−8129.
(35) Conti, I.; Garavelli, M.; Orlandi, G. The different photoisomerization efficiency of azobenzene in the lowest $n\pi^*$ and $\pi\pi^*$ singlets: the role of a phantom state. *J. Am. Chem. Soc.* **2008**, *130*, 5216−5230.
(36) Bandara, H. M. D.; Burdette, S. C. Photoisomerization in different classes of azobenzene. *Chem. Soc. Rev.* **2012**, *41*, 1809−1825.
(37) Volchkov, V. V.; Rusalov, M. V.; Gostev, F. E.; Shelaev, I. V.; Nadtochenko, V. A.; Vedernikov, A. I.; Efremova, A. A.; Kuz'mina, L. G.; Gromov, S. P.; Alfimov, M. V.; Melnikov, M. Y. Complexation of bis-crown stilbene with alkali and alkaline-earth metal cations. Ultrafast excited state dynamics of the stilbene−viologen analogue charge transfer complex. *J. Phys. Org. Chem.* **2018**, *31*, No. e3759.
(38) Vedernikov, A. I.; Kuz'mina, L. G.; Botsmanova, A. A.; Strelenko, Y. A.; Howard, J. A. K.; Alfimov, M. V.; Gromov, S. P. Stacking structures of complexes between bis(crown)azobenzene and a dipyridylethylene derivative in a crystal and in solution. *Mendeleev Commun.* **2007**, *17*, 148−150.
(39) Vedernikov, A. I.; Basok, S. S.; Gromov, S. P.; Kuz'mina, L. G.; Avakyan, V. G.; Lobova, N. A.; Kulygina, E. Yu.; Titkov, T. V.; Strelenko, Y. A.; Ivanov, E. I.; Howard, J. A. K.; Alfimov, M. V. Synthesis and structure of bis-crown-containing stilbenes. *Russ. J. Org. Chem.* **2005**, *41*, 843−854.
(40) Cacciapaglia, R.; Di Stefano, S.; Mandolini, L. The bis-barium complex of a butterfly crown ether as a phototunable supramolecular catalyst. *J. Am. Chem. Soc.* **2003**, *125*, 2224−2227.
(41) Gromov, S. P.; Ushakov, E. N.; Vedernikov, A. I.; Lobova, N. A.; Alfimov, M. V.; Strelenko, Y. A.; Whitesell, J. K.; Fox, M. A. A novel optical sensor for metal ions based on ground-state intermolecular charge-transfer complexation. *Org. Lett.* **1999**, *1*, 1697−1699.
(42) Kuz'mina, L. G.; Churakov, A. V.; Howard, J. A. K.; Vedernikov, A. I.; Lobova, N. A.; Botsmanova, A. A.; Alfimov, M.

https://dx.doi.org/10.1021/acsomega.0c03441
ACS Omega 2020, 5, 25993−26004

V.; Gromov, S. P. Structural investigation of model compounds for an acceptor component of a new type of charge-transfer complexes based on viologen analogues. Characteristic features of the molecular and supramolecular structures. *Crystallogr. Rep.* **2005**, *50*, 234−253.
(43) Gromov, S. P.; Vedernikov, A. I.; Kuz'mina, L. G.; Lobova, N. A.; Basok, S. S.; Strelenko, Y. A.; Alfimov, M. V. Stereoselective [2+2] photocycloaddition in bispseudosandwich complexes of bis(18-crown-6) stilbene with alkanediammonium ions. *Russ. Chem. Bull.* **2009**, *58*, 108−114.
(44) Ushakov, E. N.; Gromov, S. P.; Fedorova, O. A.; Pershina, Y. V.; Alfimov, M. V.; Barigelletti, F.; Flamigni, L.; Balzani, V. Sandwich-type complexes of alkaline-earth metal cations with a bisstyryl dye containing two crown ether units. *J. Phys. Chem. A* **1999**, *103*, 11188−11193.
(45) Ushakov, E. N.; Vedernikov, A. I.; Sazonov, S. K.; Kuz'mina, L. G.; Alfimov, M. V.; Howard, J. A. K.; Gromov, S. P. Synthesis and photochemical study of a supramolecular pseudodimeric complex of 4-styrylpyridinium derivatives. *Russ. Chem. Bull.* **2015**, *64*, 562−572.
(46) Frassineti, C.; Ghelli, S.; Gans, P.; Sabatini, A.; Moruzzi, M. S.; Vacca, A. Nuclear magnetic resonance as a tool for determining protonation constants of natural polyprotic bases in solution. *Anal. Biochem.* **1995**, *231*, 374−382.
(47) *SAINT*, version 6.02A; Bruker AXS, Inc.: Madison, WI, 2001.
(48) Sheldrick, G. M. Crystal structure refinement with *SHELXL*. *Acta Crystallogr., Sect. C: Struct. Chem.* **2015**, *71*, 3−8.
(49) Frisch, M. J.; Trucks, G. W.; Schlegel, H. B. et al. *Gaussian 16*, revision A.03; Gaussian, Inc.: Wallingford, CT, 2016.
(50) Zhao, Y.; Truhlar, D. G. The M06 suite of density functionals for main group thermochemistry, thermochemical kinetics, noncovalent interactions, excited states, and transition elements: two new functionals and systematic testing of four M06-class functionals and 12 other functionals. *Theor. Chem. Acc.* **2008**, *120*, 215−241.
(51) Hehre, W. J.; Ditchfield, R.; Pople, J. A. Self-consistent molecular orbital methods. XII. Further extensions of Gaussian-type basis sets for use in molecular orbital studies of organic molecules. *J. Chem. Phys.* **1972**, *56*, 2257−2261.
(52) Hariharan, P. C.; Pople, J. A. The influence of polarization functions on molecular orbital hydrogenation energies. *Theor. Chim. Acta* **1973**, *28*, 213−222.
(53) Marenich, A. V.; Cramer, C. J.; Truhlar, D. G. Universal solvation model based on solute electron density and on a continuum model of the solvent defined by the bulk dielectric constant and atomic surface tensions. *J. Phys. Chem. B* **2009**, *113*, 6378−6396.
(54) Kesharwani, M. K.; Brauer, B.; Martin, J. M. L. Frequency and zero-point vibrational energy scale factors for double-hybrid density functionals (and other selected methods): can anharmonic force fields be avoided? *J. Phys. Chem. A* **2015**, *119*, 1701−1714.
(55) Krishnan, R.; Binkley, J. S.; Seeger, R.; Pople, J. A. Self-consistent molecular orbital methods. XX. A basis set for correlated wave functions. *J. Chem. Phys.* **1980**, *72*, 650−654.
(56) Frisch, M. J.; Pople, J. A.; Binkley, J. S. Self-consistent molecular orbital methods 25. Supplementary functions for Gaussian basis sets. *J. Chem. Phys.* **1984**, *80*, 3265−3269.
(57) Yanai, T.; Tew, D. P.; Handy, N. C. A new hybrid exchange−correlation functional using the Coulomb-attenuating method (CAM-B3LYP). *Chem. Phys. Lett.* **2004**, *393*, 51−57.

https://dx.doi.org/10.1021/acsomega.0c03441
ACS Omega 2020, 5, 25993−26004